Whether the 'superlattice' spots correspond to the **a** axis of the true unit cell [as the 12:7 case was reported to be by Graham *et al.* (1953)] or only to one of the large subcells proposed by Matzat cannot be determined definitively from these measurements which, at ±1%, are insufficiently precise. The enlargements, Figs. 6(*a'–c'*), do not help in this respect. That the intervals 17/10 and 12/7 dominate the diffraction patterns (irrespective of the exact measurements), and that there are no additional (more closely spaced) reflections, strongly suggests that each true structure is (at least) dominated by one of these substructures. Since our selected-area diffraction patterns come from very small volumes of crystal (compared with that required for X-ray diffraction) it may well be that the two substructures are true (local) structures; and that a large crystal (as used for X-ray diffraction) may be a heterogeneous mixture of the two. Certainly there is no evidence here for the larger cell, $46 \times a_T = 27 \times a_O$, reported by Matzat.

This implies that the stoichiometries are 17PbS.-$10Bi_2S_3$ for (*a,a'*) and $12PbS.7Bi_2S_3$ for (*b,b'*) and (*c,c'*), *i.e.* $\sim PbBi_{1.176}S_{2.765}$ and $\sim PbBi_{1.167}S_{2.750}$ instead of Matzat's $\sim PbBi_{1.174}S_{2.761}$. Again these are very small variations: only ~0·2% and ~0·6% for Bi, and ~0·1% and ~0·4% for S (relative to Pb).

Concluding remarks

In the 'LnMS_3' cases we again find no evidence of disorder [*cf.* Otero-Diaz *et al.* (1985)], apart from twinning on (001). The variation in the b_T/b_O mismatch with change in Ln and/or *M* seems to us to support the earlier suggestion (Otero-Diaz *et al.*, 1985) that there is no other disorder (*e.g.* empty Ln sites or *M* on Ln sites). It follows that none of these has stoichiometry LnMS_3, but rather $\sim Ln_{1.2}MS_{3.2}$.

In synthetic and natural cannizzarite we find the two basic, layer mismatches $a_O/a_T = 12/7$ and 17/10, but no evidence for their combinations $46/27 = (12 + 2 \times 17)/(7 + 2 \times 10)$ or $41/24 = (2 \times 12 + 17)/(2 \times 7 + 10)$, as proposed by Matzat (1979).

References

BESANÇON, P. (1973). *J. Solid State Chem.* **7**, 232–240.

BESANÇON, P., CARRÉ, D. & LARUELLE, P. (1973). *Acta Cryst.* B**29**, 1064–1066.

DONOHUE, P. C. (1975). *J. Solid State Chem.* **12**, 80–83.

GRAHAM, A. R., THOMPSON, R. M. & BERRY, L. G. (1953). *Am. Mineral.* **38**, 536–544.

KATO, K., KAWADA, I. & TAKAHASHI, T. (1977). *Acta Cryst.* B**33**, 3437–3443.

MAKOVICKY, E. & HYDE, B. G. (1981). *Struct. Bonding (Berlin)*, **46**, 101–170.

MATZAT, E. (1979). *Acta Cryst.* B**35**, 133–136.

MURUGESAN, T., RAMESH, S., GOPALAKRISHNAN, J. & RAO, C. N. R. (1981). *J. Solid State Chem.* **38**, 165–172.

OTERO-DIAZ, L., FITZ GERALD, J. D., WILLIAMS, T. B. & HYDE, B. G. (1985). *Acta Cryst.* B**41**, 405–410.

SEREBRENNIKOV, V. V. & ALEKSEEVA, T. P. (1981). *Russ. J. Inorg. Chem.* **26**, 837–838.

TAKAHASHI, T., OKA, T., YAMADA, O. & AMETAMI, K. (1971). *Mater. Res. Bull.* **6**, 173–182.

TAKAHASHI, T., OSAKA, S. & YAMADA, O. (1973). *J. Phys. Chem. Solids*, **34**, 1131–1135.

WILLIAMS, T. B. & HYDE, B. G. (1988). *Phys. Chem. Miner.* In the press.

ZAMBONINI, F., DE FIORE, O. & CAROBBI, G. (1925). *Rend. Accad. Sci. Fis. Nat. Naples Ser.* 3, **31**, 24–29.

Acta Cryst. (1988). B**44**, 474–480

A New Pseudo-Binary Tungsten Oxide, $W_{17}O_{47}$

BY M. M. DOBSON AND R. J. D. TILLEY

Department of Materials, University College, Newport Road, Cardiff CF2 1TA, Wales

(*Received* 22 *January* 1986; *accepted* 8 *April* 1988)

Abstract

A new pseudo-binary tungsten oxide which has the composition $W_{17}O_{47}$ ($WO_{2.765}$) has been discovered in the Sb–W–O system. The phase is stable up to about 1233 K and decomposes to $W_{18}O_{49}$ and $W_{24}O_{28}$ above this temperature. The approximate structure has been determined by high-resolution electron microscopy and powder X-ray diffraction methods. The monoclinic unit-cell parameters are $a = 18{\cdot}84$, $b = 3{\cdot}787$, $c = 12{\cdot}33$ Å, $\beta = 102{\cdot}67°$, $Z = 1$, space group $P2/m$. The structure is built up of octahedra and pentagonal columns linked in such a way as to form hexagonal tunnels.

Introduction

Tungsten trioxide has a crystal structure which can be described as being built up from slightly distorted octahedra arranged so as to share corners. Reduction of WO_3 to compositions below approximately $WO_{2.87}$ results in the formation of structures which are built up from WO_7

0108-7681/88/050474-07$03.00

pentagonal bipyramids surrounded by five edge-sharing octahedra. This structural component is often referred to as a pentagonal column (PC) unit. Each PC has an effective stoichiometry of $WO_{2.667}$. In the binary tungsten–oxygen system two PC-containing phases are known to exist, namely $W_{24}O_{68}$ (Sundberg, 1978) and $W_{18}O_{49}$ (Magnéli, 1949). In addition a pseudo-binary oxide of formula W_5O_{14} can be stabilized by small amounts of several ternary metals (Ekström & Tilley, 1976).

Although much progress has been made towards understanding the crystal chemistry of the binary and pseudo-binary tungsten oxides, the reasons for the complexity and variety of phases which form are still not fully understood. This has been emphasized by the discovery of another pseudo-binary oxide discovered during an investigation into the Sb–W–O system. The approximate structure of this phase, deduced with the aid of high-resolution electron microscopy, is reported here.

Experimental

Compositions in the Sb–W–O system along the Sb_xWO_3 line in the phase diagram were prepared by mixing appropriate amounts of 'Specpure'-grade Sb metal and WO_3 (Johnson Matthey Ltd). The compositions prepared that are relevant to the present paper corresponded to $x = 0{\cdot}15$, $0{\cdot}19$, $0{\cdot}21$ and $0{\cdot}25$. The mixtures were sealed into evacuated silica tubes and positioned vertically in a muffle furnace. The samples were heated for 4–7 days at 1223 or 1423 K before being removed and quenched in liquid nitrogen.

X-ray analysis of the products was carried out using a Hägg–Guinier focusing camera using strictly monochromatic Cu $K\alpha_1$ radiation and KCl ($a = 6{\cdot}292$ Å) as an internal standard. The resulting X-ray powder diffraction patterns were measured using an eyepiece and 0·1 mm scale exposed on the film before development to compensate for film shrinkage. Refinement of unit-cell data was performed using computer programs utilizing least-squares methods to determine lattice parameters (Nord, 1963; Werner, 1969). X-ray powder pattern intensities were estimated by using a Joyce–Loebl densitometer and calculated using a program written by Yvon, Jeitschko & Parthé (1977).

A Jeol 200CX transmission electron microscope was used to obtain high-resolution images of suitably oriented fragments. Samples for microscopy were prepared by crushing a single crystal of the sample in an agate mortar under *n*-butanol. A drop of the resulting suspension was placed on a holey carbon support film and allowed to evaporate. High-resolution images were obtained by precisely aligning thin crystal flakes projecting over holes in the carbon support films so that the short unit-cell axis, *i.e.* the *b* axis of the monoclinic unit, was parallel to the incident electron beam. Images were obtained by under-focusing by approximately 60 nm and taking through-focal series at 9 nm increments. Images were recorded at direct magnifications of 500 000 × to 1 000 000 ×. The objective lens had a C_s of 1·2 mm and the objective aperture, which was used to exclude reflections with large scattering angles, had a radius of 0·35 nm in reciprocal space. Computed images for a range of defocus and thickness values were calculated on the Honeywell DPS-8/70M computer of the Joint Cardiff Computing Service, employing programs *FCOEFF* and *DEFECT* written by Skarnulis (1976). The depth of focus owing to chromatic aberration was assumed to be 20 nm.

Chemical analysis was carried out on a JSM 35CF scanning electron microscope fitted with a Link Systems 860 Series 2 energy-dispersive-analysis system. The microscope was operated at 21 kV and the diameter of the probe was estimated to be 1–2 μm. Results were corrected for atomic number, absorption and fluorescence errors using the Link System ZAF-4/FLS computer routine. Individual analyses were accurate to between 0·1–0·2 at.%. In addition, morphological observations were also carried out on this instrument.

Oxidation experiments were carried out on a Sartorius 4102 microbalance capable of registering weight changes in the μg region. Before each experiment the balance was standardized and the sample weighed in vacuum. The sample was oxidized at 933 K until constant weight was achieved and again weighed in vacuum.

Results

During investigations into the Sb–W–O system, metallic mauve–pink lathlike crystals were found in a number of preparations of bulk composition Sb_xWO_3 reacted at 1233 K. These crystals, which ranged in size from 1–5 mm long × 0·1 mm wide, were found both on the surface and embedded in the blue crystals of the bulk material, and comprised only a fraction of the samples. Scanning electron microscopy revealed that each lath was composed of many smaller similarly shaped crystals of needlelike habit, as shown in Fig. 1. These needlelike crystals are stacked parallel to each other, so as to form an apparently platey crystal. Attempts to prepare monophasic samples by varying both the overall composition of the preparations or the heating times and temperatures were not successful.

A further series of experiments carried out with the same Sb contents but at the higher reaction temperature of 1423 K did not produce these crystals, indicating that they were unstable at higher temperatures. This was confirmed by sealing small quantities of the crystals in evacuated silica ampoules which were

subsequently heated at 1373 K for 5 days. After reaction, it was found that the original crystals had decomposed. In their place, approximately equal amounts of extremely fine needlelike crystals, one of which was blue and the other mauve, had formed on the sides of the tubes. The X-ray diffraction pattern obtained from the mauve material was identical to that of the binary oxide $W_{18}O_{49}$ whilst the blue phase gave a diffraction pattern identical to that of $W_{24}O_{68}$. These results suggested that the unknown material might be a binary or pseudo-binary tungsten oxide with a composition somewhere between $WO_{2.72}$ and $WO_{2.82}$.

Although monophasic preparations were not achieved, X-ray powder diffraction patterns of these metallic crystals were obtained by manually separating surface crystals and crushing them onto the tape used in the X-ray sample holder. Details of the powder pattern are listed in Table 1. It should be noted that the lathlike nature of the crystals and the method of preparing the X-ray specimens from rather limited quantities of material may result in preferred orientation effects, and the visual intensities recorded in Table 1 should be used only as a guide. Despite this limitation it was apparent that the powder pattern could not be assigned to any previously characterized phase in either the Sb–W–O system or the binary W–O system.

Electron diffraction patterns recorded from crystal fragments showed that in every case the reflections were sharp and no diffuse scattering was observed, indicating that the crystals were well ordered. A typical electron diffraction pattern is shown in Fig. 2. Approximate values for the unit-cell dimensions of the phase were obtained from these electron diffraction patterns which also suggested that the symmetry was monoclinic. The values found were $a = 18{\cdot}8$, $b = 3{\cdot}8$, $c = 12{\cdot}4$ Å and $\beta = 102°$, for the monoclinic cell. These values were used to index the powder X-ray data to yield refined values for the lattice constants of $a = 18{\cdot}84\ (2)$, $b = 3{\cdot}787\ (5)$, $c = 12{\cdot}326\ (7)$ Å and $\beta = 102{\cdot}67\ (1)°$. The observed and calculated d spacings and $\sin^2\theta$ values for the reflections are listed in Table 1.

Electron probe microanalysis was used in an attempt to determine the compositions of the crystals. Numerous analyses revealed no trace of Sb, indicating that the amount present must be less than 0·2 at.%, which was the detection limit of the instrument. As oxygen content could not be accurately determined by this method, the tungsten-to-oxygen composition was obtained by oxidizing the crystals and measuring the weight increase. The final product of the oxidation was determined, by powder X-ray diffraction, to be WO_3. The weight increase then yielded a composition of $WO_{2.80}$ for the crystals.

To obtain a model for the structure, high-resolution electron microscope images were utilized. An image from a typical fragment, shown in the low-magnification micrograph of Fig. 3, reveals that the phase is well ordered. Indeed, faulting or other structural disorder was never observed over large areas of some 20 crystals examined.

A high-magnification image is shown in Fig. 4. The unit cell of the material is readily detected, and is outlined on the micrograph. In such images the most obvious features were the existence of groups of three white spots arranged in zigzag chains. Between the top of one group of three white spots and the bottom of another group in the zigzag chain there is a large white spot. This type of contrast is typical of two pentagonal column units joined by edge sharing to create two empty pentagonal column units separated by one empty

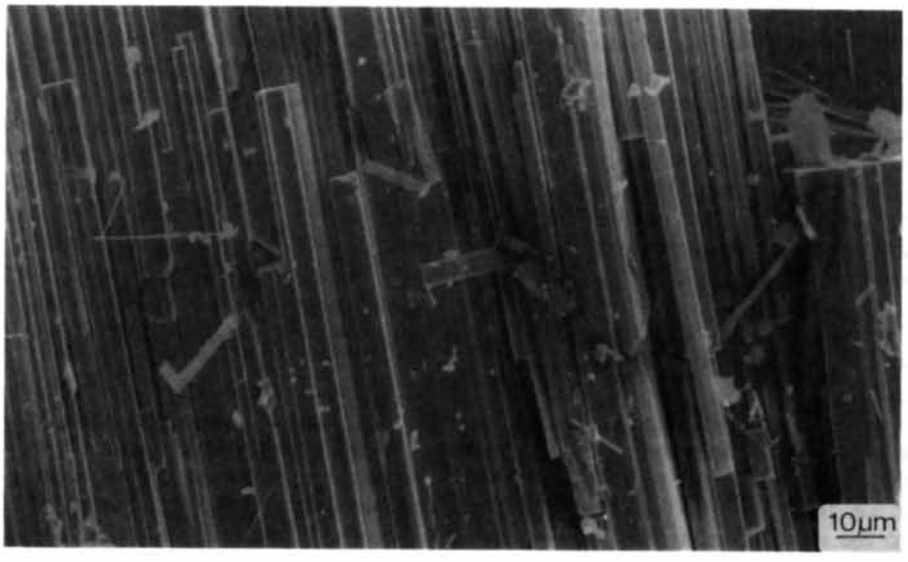

Fig. 1. Scanning electron micrograph of lathlike pink metallic crystals obtained from a sample of $Sb_{0.19}WO_3$. The crystals are composed of numerous needlelike fragments arranged parallel to each other so as to form an apparently platey crystal.

Table 1. *Observed and calculated powder X-ray diffraction data for* $W_{17}O_{47}$

$I_{obs.}$	$d_{obs.}$	$d_{calc.}$	$\sin^2\theta_{obs.}$	$\sin^2\theta_{calc.}$	hkl	Δ^*
4	9·132	9·189	0·00711	0·00703	200	9
1	6·619	6·633	0·01354	0·01349	201	6
1	6·007	6·013	0·01644	0·01641	002	3
2	5·608	5·629	0·01887	0·01872	−202	14
5	5·367	5·377	0·02060	0·02052	102	7
6	4·115	4·112	0·03504	0·03509	−402	−5
22	4·009	4·009	0·03691	0·3692	003	1
100	3·787	3·787	0·04137	0·04137	010	0
6	3·750	3·749	0·04218	0·04221	103	3
1	3·676	3·675	0·04390	0·4392	500	2
2	3·590	3·590	0·04605	0·04605	−111	0
8	3·496	3·496	0·04854	0·04855	−502	1
16	3·410	3·410	0·05103	0·05102	203	1
4	3·314	3·326	0·05402	0·05394	402	8
6	3·287	3·289	0·05493	0·05485	211	7
4	3·220	3·221	0·05722	0·05718	310	4
4	3·095	3·096	0·06193	0·06189	112	4
4	3·077	3·077	0·06265	0·06268	−104	−3
5	3·066	3·065	0·06313	0·06317	−503	−3
4	3·061	3·061	0·06333	0·06334	303	−1
14	3·005	3·006	0·06570	0·06564	004	6
36	2·969	2·969	0·06731	0·06731	−304	0
5	2·869	2·868	0·07207	0·07211	104	−4
9	2·815	2·815	0·07488	0·07489	−404	−2
5	2·787	2·786	0·07638	0·07646	−412	−8
25	2·751	2·753	0·07837	0·07829	411	8

The refined dimensions of the monoclinic unit cell are: $a = 18{\cdot}84$, $b = 3{\cdot}787$, $c = 12{\cdot}326$ Å, $\beta = 102{\cdot}67°$.

* $\Delta = (\sin^2\theta_{obs.} - \sin^2\theta_{calc.}) \times 10^5$.

octahedron (Sundberg, 1978). Contrast identical to that shown by the larger white spot has been consistently interpretated in the past as being due to a hexagonal tunnel (Pickering & Tilley, 1976; Ekström & Tilley, 1976). In the image it was also possible to observe a distorted row of eight octahedra joining the bottom white spot of one group of three to the upper white spot of the next group of three in the zigzag chain.

Despite uncertainties inherent in the direct determination of structures from high-resolution images, these clues seemed sufficient to deduce likely structures for the phase. Constructing the unit cell from these basic structural features we arrived at the structure shown in Fig. 5. The unit cell of the phase is identical to that derived by powder X-ray diffraction and the unit-cell contents yield a composition of $W_{17}O_{47}$, that is, $WO_{2.765}$.

To quantify matters, computed images were calculated from the structural model shown in Fig. 5. The positions of the atoms used in this simulation are given

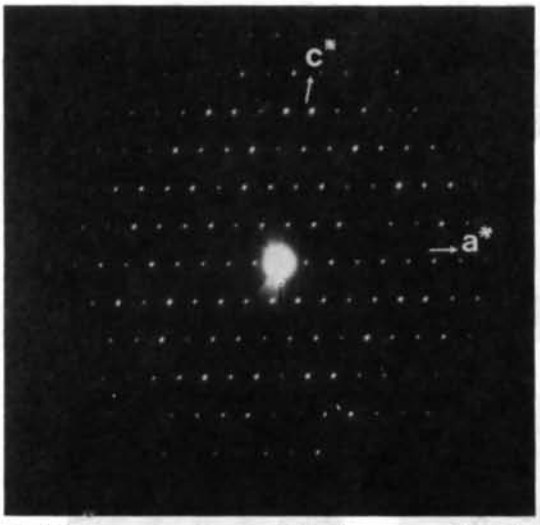

Fig. 2. [010]-zone-axis electron diffraction pattern from lathlike crystals obtained from a sample of bulk composition $Sb_{0.19}WO_3$.

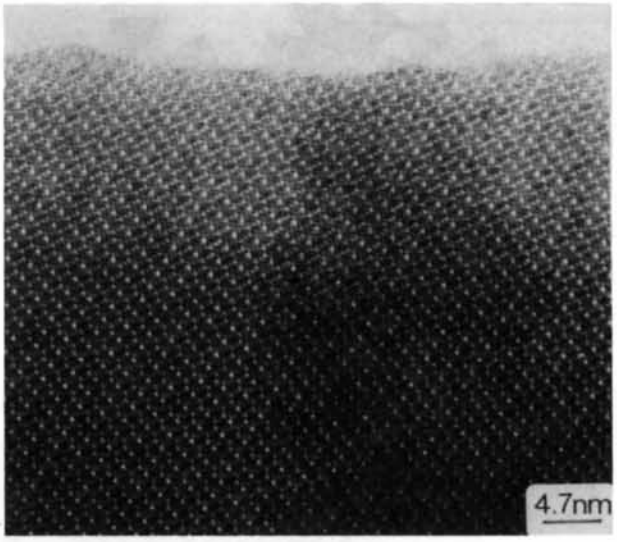

Fig. 3. Low-magnification image, projected down [010], of a typically well-ordered crystal.

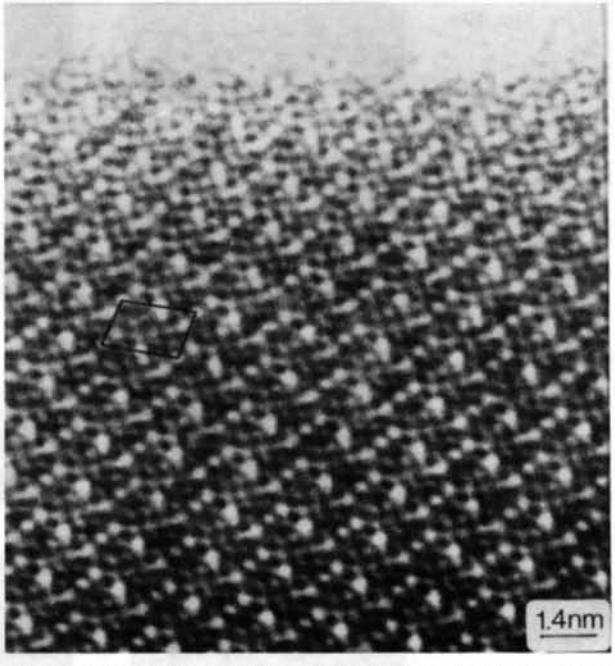

Fig. 4. High-magnification image, projected down [010], of a typical crystal. The unit cell is outlined. Note the zigzag pattern of white spots representing empty tunnels in the structure.

in Table 2. Figs. 6(*a–g*) show a series of images obtained for different defocus values and crystal thicknesses. The optimum defocus value is close to −67 nm. The structure images obtained agree well with calculated images for crystal thicknesses of up to 10 slices, each of thickness equal to the *b* parameter, and are in complete agreement with the suggested model.

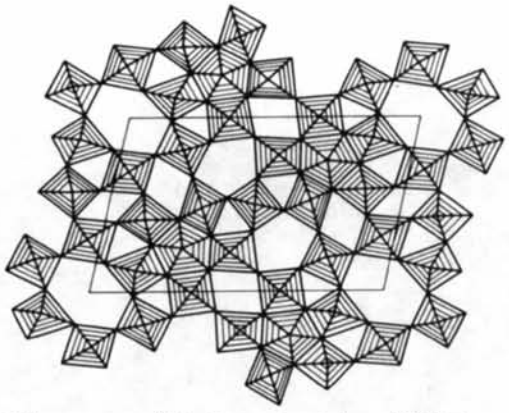

Fig. 5. The structure of $W_{17}O_{47}$ projected down [010]. The unit cell is outlined.

Table 2. *Atomic coordinates of the atoms in* $W_{17}O_{47}$

Space group $P2/m$, $Z = 1$.

	x	*y*	*z*
W1	0·657	0·0	0·000
W2	0·791	0·0	0·819
W3	0·679	0·0	0·468
W4	0·950	0·0	0·665
W5	0·873	0·0	0·425
W6	0·541	0·0	0·213
W7	0·705	0·0	0·241
W8	0·858	0·0	0·128
W9	0·500	0·0	0·500
O1	0·657	0·5	0·000
O2	0·791	0·5	0·819
O3	0·679	0·5	0·468
O4	0·950	0·5	0·665
O5	0·873	0·5	0·425
O6	0·541	0·5	0·213
O7	0·705	0·5	0·241
O8	0·858	0·5	0·128
O9	0·500	0·5	0·500
O10	0·560	0·0	0·883
O11	0·524	0·0	0·644
O12	0·596	0·0	0·525
O13	0·724	0·0	0·665
O14	0·697	0·0	0·867
O15	0·739	0·0	0·414
O16	0·623	0·0	0·298
O17	0·593	0·0	0·117
O18	0·754	0·0	0·095
O19	0·828	0·0	0·266
O20	0·875	0·0	0·570
O21	0·966	0·0	0·442
O22	0·855	0·0	0·990
O23	0·873	0·0	0·782
O24	0·029	0·0	0·809

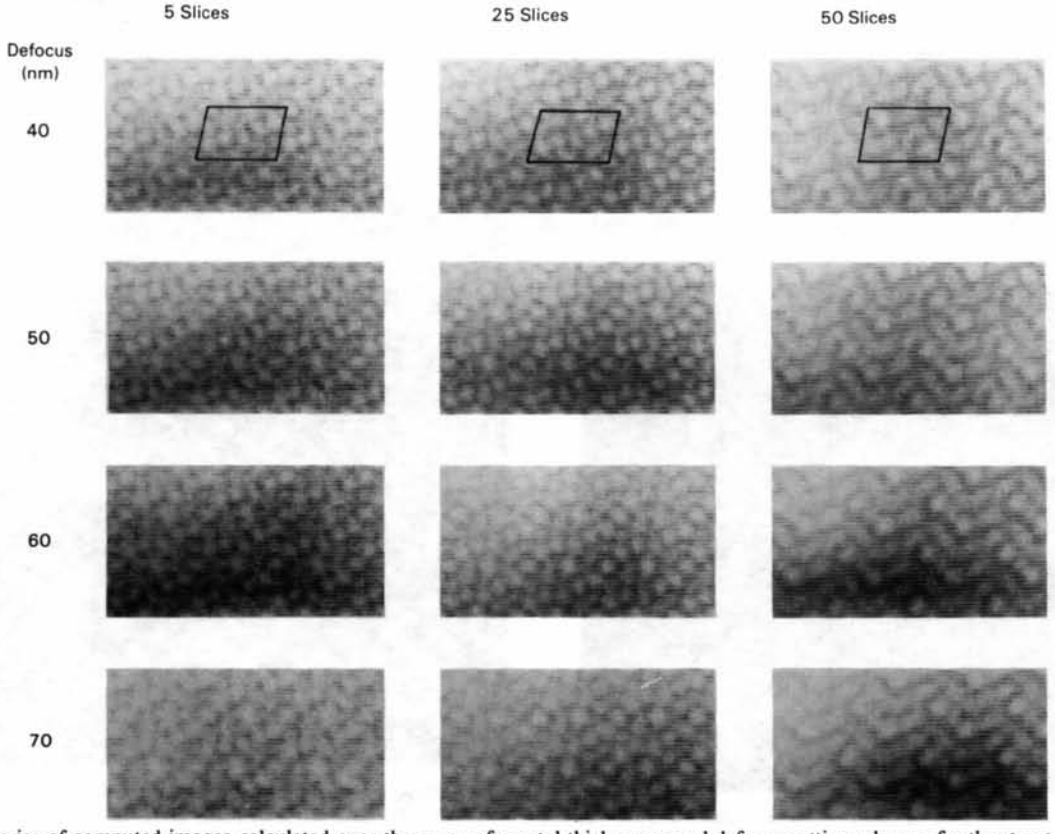

Fig. 6. A series of computed images calculated over the range of crystal thicknesses and defocus settings shown, for the structure in Fig. 5.

Discussion

It has been known for some time that by careful choice of imaging conditions it is possible to interpret the observed contrast of a high-resolution electron micrograph in terms of the projected charge density of the object in which white areas represent holes in the structure and black regions represent heavy-metal atoms. We have been careful to reproduce these conditions before obtaining the images used in the interpretation resulting in Fig. 5. The accurate correlation between the through-focal series of images obtained experimentally and that obtained *via* calculations over large ranges of focus gives confidence to the belief that the proposed structure is essentially correct.

Although the phase has a suggested composition of $W_{17}O_{47}$, it does not appear to occur in the binary W—O system. It therefore seems to be a pseudo-binary oxide stabilized by the presence of antimony. In this respect it is similar to W_5O_{14}, which is also only stabilized by the presence of impurity metals in the preparations (Ekström & Tilley, 1976). By analogy with this latter phase, we would expect that $W_{17}O_{47}$ would also be stabilized by other metal impurities, and a systematic search would be of interest.

This has partly been verified by the report of Sundberg & Lundberg (1987) which was published during preparation of this paper. Sundberg & Lundberg report on the structures of a series of compounds $K_x(Nb,W)_{17}O_{47}$, in which x takes values of between 1 and 2. It is immediately clear that the framework of these phases is identical to the structure for $W_{17}O_{47}$ that we have suggested. The unit-cell parameters are also close to those reported here, and reflect the identity of the two frameworks involved.

The new oxide has a composition which places it close to the known phases $W_{24}O_{68}$ ($WO_{2.833}$), W_5O_{14} ($WO_{2.80}$) and $W_{18}O_{49}$ ($WO_{2.72}$), and the phase incorporates some of the features of all these oxides, as can be seen by comparison with Fig. 7. The relationship with the $W_{18}O_{49}$ structure is quite marked. In both of these structures groups of two PC units link in a manner so as to form a hexagonal tunnel (HT), the PC–HT–PC unit of Sahle & Sundberg (1980). However, a notable difference occurs between the way in which these groups are linked in the two compounds. In $W_{17}O_{47}$

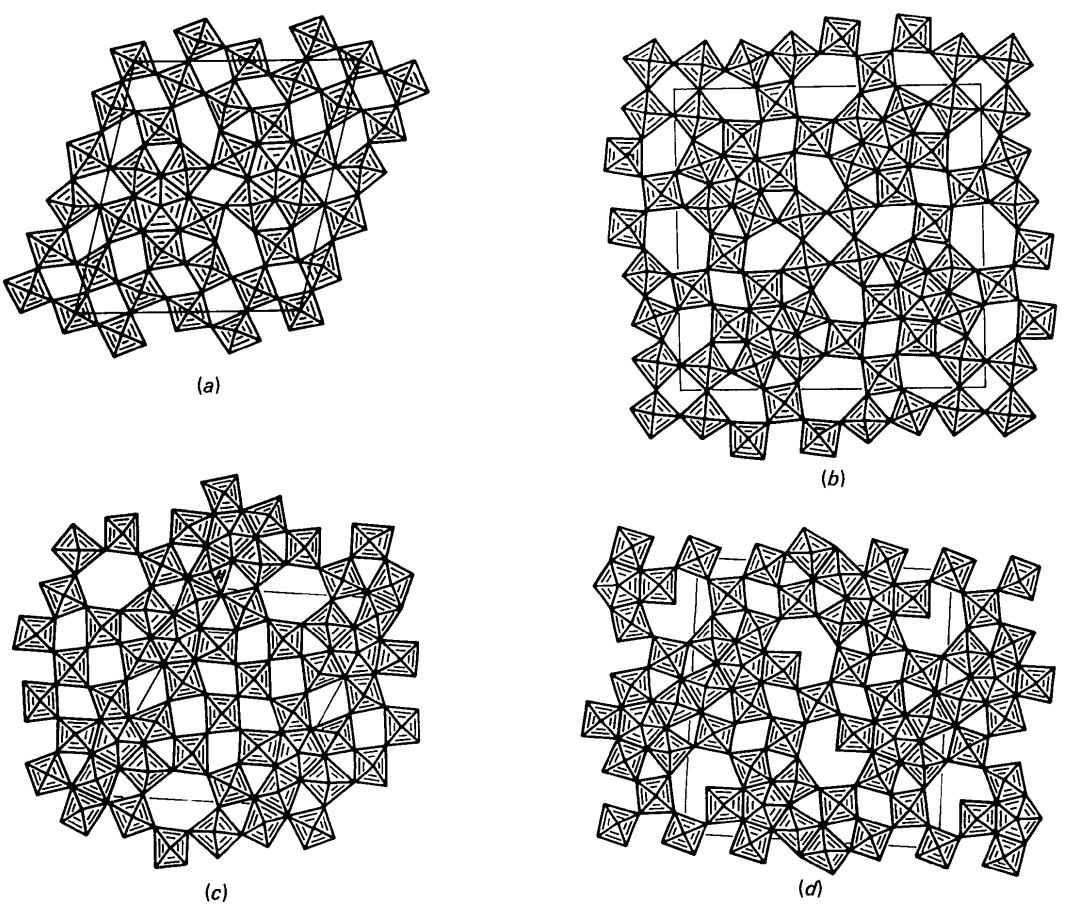

Fig. 7. The crystal structures of (*a*) $W_{24}O_{68}$, (*b*) W_5O_{14}, (*c*) $W_{18}O_{49}$ and (*d*) $Mo_{17}O_{47}$. All structures are projected down the short axis in the structure, equivalent to one WO_6 octahedron diagonal.

these units are linked only by corner sharing of octahedra, whilst in $W_{18}O_{49}$ edge sharing also occurs. It is this feature that reduces the oxygen-to-metal ratio in this latter phase compared to $W_{17}O_{47}$. A comparison with the oxide $W_{24}O_{68}$ is also marked and the connectivity within a group of 24 polyhedra is the same in both structures.

It is interesting to note that the molybdenum oxide of equivalent composition, $Mo_{17}O_{47}$, has the somewhat different, but related structure (Kihlborg, 1960, 1963) shown in Fig. 7(*d*). Here the MoO_7 pentagonal bipyramids are joined together by edge sharing, resembling the arrangement in $W_{18}O_{49}$. In the Mo oxide, however, the hexagonal tunnels are blocked by O atoms. By comparison, it is apparent that $Mo_{17}O_{47}$ is more closely related structurally to $W_{18}O_{49}$ than to its compositional equivalent $W_{17}O_{47}$.

The present study has elucidated, by high-resolution electron microscopy, the likely structure of a new tungsten oxide. It forms in the presence of Sb and in this respect can be compared with the pseudo-binary oxide W_5O_{14}. It seems possible, therefore, that these materials form part of a series of related phases which are only stable over narrow ranges of temperature and composition in the presence of one or more ternary metals. A comprehensive search for other new phases would be of interest. Such a study, as well as a refinement of the structure of the phase described in this paper, will be reported in future communications.

MMD is indebted to ICI New Science Group, Runcorn, Cheshire, for financial support.

References

EKSTRÖM, T. & TILLEY, R. J. D. (1976). *J. Solid State Chem.* **19**, 125–133.

KIHLBORG, L. (1960). *Acta Chem. Scand.* **14**, 1612–1622.

KIHLBORG, L. (1963). *Acta Chem. Scand.* **17**, 1485–1487.

MAGNÉLI, A. (1949). *Ark. Kemi*, **1**, 223–230.

NORD, A. G. (1963). Dissertation, Univ. of Stockholm, Sweden.

PICKERING, R. & TILLEY, R. J. D. (1976). *J. Solid State Chem.* **16**, 247–255.

SAHLE, W. & SUNDBERG, M. (1980). *Chem. Scr.* **16**, 163–168.

SKARNULIS, A. J. (1976). PhD Thesis, Arizona State Univ., USA.

SUNDBERG, M. (1978). *Chem. Scr.* **14**, 161–166.

SUNDBERG, M. & LUNDBERG, M. (1987). *Acta Cryst.* B**43**, 429–434.

WERNER, P. E. (1969). *Ark. Kemi*, **31**, 513–516.

YVON, K., JEITSCHKO, W. & PARTHÉ, E. (1977). *J. Appl. Cryst.* **10**, 73–74.

Acta Cryst. (1988). B**44**, 480–486

Structure of Al_mFe

BY PER SKJERPE

Department of Physics, University of Oslo, PO Box 1048, *Blindern* 0316, *Oslo* 3, *Norway*

(*Received* 27 *October* 1987; *accepted* 28 *April* 1988)

Abstract

The metastable phase Al_mFe ($m = 4{\cdot}0$–$4{\cdot}4$, body-centred tetragonal, $a = 8{\cdot}84$, $c = 21{\cdot}6$ Å) has been examined by transmission electron microscopy and high-resolution electron microscopy (HREM). Crystals, 1–10 μm in size, were extracted from a cast Al–0·25wt%Fe–0·13wt%Si alloy of commercial purity. By the use of electron diffraction patterns, a possible structure model for Al_mFe was set up, assuming space group *I*4/*mmm*. The model was in qualitative agreement with diffraction patterns as well as HREM micrographs, recorded in ⟨100⟩ and ⟨110⟩. Streaks along *hh*0 in the diffraction patterns were ascribed to faults on (110).

1. Introduction

Iron and silicon are always present in commercial aluminium alloys and primary particles of Al–Fe and Al–Fe–Si are usually precipitated during casting. The particle types appearing depend on alloy composition (Fe/Si ratio) and the cooling rate during solidification. Low cooling rates favour formation of equilibrium phases, higher cooling rates cause metastable Al–Fe(–Si) phases to be formed (Westengen, 1982).

The crystal structures of most equilibrium Al–Fe–Si phases have been determined (Black, 1955*a*,*b*; Walford, 1965; Cooper, 1967; Cooper & Robinson, 1966; Corby & Black, 1977). On the other hand, the structures of most metastable Al–Fe–Si phases are not known, except approximate lattice parameters and chemical compositions. X-ray diffraction studies of these particles encounter difficulties; the crystals are a few micrometres in size and usually a mixture of phases will be contained in the ingot. Thus transmission electron microscopy (TEM) is essential for analyzing the structure of these particles.

During a TEM study of particles in a cast Al–Fe–Si alloy (Skjerpe, 1987), one of the metastable phases

0108-7681/88/050480-07$03.00